Molecular Cancer Therapeutics

CAT-02-106, a Site-Specifically Conjugated Anti-CD22 Antibody Bearing an MDR1-Resistant Maytansine Payload Yields Excellent Efficacy and Safety in Preclinical Models

Penelope M. Drake, Adam Carlson, Jesse M. McFarland, Stefanie Bañas, Robyn M. Barfield, Wesley Zmolek, Yun Cheol Kim, Betty C.B. Huang, Romas Kudirka, and David Rabuka

Abstract

Hematologically derived tumors make up ~10% of all newly diagnosed cancer cases in the United States. Of these, the non-Hodgkin lymphoma (NHL) designation describes a diverse group of cancers that collectively rank among the top 10 most commonly diagnosed cancers worldwide. Although long-term survival trends are improving, there remains a significant unmet clinical need for treatments to help patients with relapsed or refractory disease, one cause of which is drug efflux through upregulation of xenobiotic pumps, such as MDR1. CD22 is a clinically validated target for the treatment of NHL, but no anti-CD22 agents have yet been approved for this indication. Recent approval of an anti-CD22 antibody–drug conjugate (ADC) for the treatment of relapsed/refractory ALL supports the rationale for targeting this protein. An opportunity exists for a next-generation anti-CD22 antibody–drug conjugate (ADC) to address unmet medical needs in the relapsed/refractory NHL population. We describe a site-specifically conjugated antibody–drug conjugate, made using aldehyde tag technology, targeted against CD22 and bearing a noncleavable maytansine payload that is resistant to MDR1-mediated efflux. The construct was efficacious against $CD22^+$ NHL xenografts and could be repeatedly dosed in cynomolgus monkeys at 60 mg/kg with no observed significantly adverse effects. Exposure to total ADC at these doses (as assessed by $AUC_{0\text{-inf}}$) indicated that the exposure needed to achieve efficacy was below tolerable limits. Together, the data suggest that this drug has the potential to be used effectively in patients with $CD22^+$ tumors that have developed MDR1-related resistance to prior therapies. *Mol Cancer Ther; 17(1); 161–8. ©2017 AACR.*

Introduction

Leukemias, lymphomas, and myelomas are highly prevalent in the population, accounting for ~10% of all newly diagnosed cancer cases in the United States during 2015 (1). Of these cancers, B-cell–derived malignancies comprise a large and diverse group that includes non-Hodgkin lymphoma (NHL), chronic lymphocytic leukemia (CLL), acute myeloid leukemia (AML), and acute lymphoblastic leukemia (ALL). Similarly, as a category, NHL designates about 60 lymphoma subsets, of which about 85% are B-cell derived, including diffuse large B-cell lymphoma (DLBCL), follicular lymphoma (FL), and mantle cell lymphoma (MCL). Collectively, NHL diseases are among the most common cancer types observed, ranking as the seventh most common cancer in the United States (1), and the 10th most common cancer diagnosed worldwide in 2012 (2–4). While long-term trends show improvements in 5-year survival rates for most blood cancer diagnoses, there remains a significant unmet clinical need, with 16% of CLL, 30% of ALL, and 30% of NHL patients diagnosed from 2004 to 2010 failing to meet the 5-year survival endpoint (1).

CD22 is a B-cell lineage-restricted cell surface glycoprotein that is expressed on the majority of B-cell hematologic malignancies, but is not expressed on hematopoietic stem cells, memory B cells, or other normal nonhematopoietic tissues (5, 6). Its expression pattern and rapid internalization kinetics make it a promising target for antibody–drug conjugate (ADC) therapies, and it has been tested as such in several clinical trials against NHL and ALL. The most advanced clinical candidate in this area is inotuzumab ozogamicin (ref. 7; Pfizer), an anti-CD22 antibody conjugated through lysine residues to calicheamicin, a potent DNA-damaging agent. Inotuzumab ozogamicin has been tested in phase III trials enrolling patients with either NHL or ALL. Although the drug failed to improve overall survival for either patient group, it met the primary endpoint of a higher complete hematologic remission rate for ALL patients and also extended the progression-free survival in this group (8). On the basis of these results, the drug—branded as Besponsa—was recently approved by both the FDA and EMA for treatment of relapsed/refractory ALL. These regulatory achievements validate CD22 as a clinical target for ADCs designed to treat $CD22^+$ hematological malignancies. Another anti-CD22 ADC, pinatuzumab vedotin (Genentech/Roche) is

Catalent Biologics, Emeryville, California.

Note: Supplementary data for this article are available at Molecular Cancer Therapeutics Online (http://mct.aacrjournals.org/).

Corresponding Author: David Rabuka, Catalent Biologics, 5703 Hollis Street, Emeryville, CA 94608. Phone: 510-343-6031; Fax: 510-225-3949; E-mail: david.rabuka@catalent.com

doi: 10.1158/1535-7163.MCT-17-0776

conjugated through endogenous cysteine residues to the microtubule-binding auristatin, MMAE (9). Pinatuzumab vedotin's efficacy was tested against that of a related ADC targeting the B-cell marker CD79b in a phase II trial in patients with NHL (10). Although pinatuzumab vedotin treatment returned promising results, with an overall response rate of 57%, its development was discontinued in favor of pursuing the alternate candidate.

Here, we describe an anti-CD22 ADC—CAT-02-106—that builds on and extends this previous work. We use site-specific conjugation technology based upon the aldehyde tag (11) and HIPS chemistry (12) to place a maytansine payload coupled through a noncleavable linker to the antibody heavy chain *C*-terminus. The genetically encoded aldehyde tag incorporates the six amino acid sequence, LCTPSR. Cotranslationally, overexpressed formylglycine generating enzyme converts the cysteine within the consensus sequence to a formylglycine residue (13), bearing an aldehyde functional group, which is reacted with a HIPS-linker-payload to generate an ADC (14). This approach affords control over both payload placement and DAR and yields highly homogenous ADC preparations. Previous studies have indicated that site-specifically conjugated ADCs display improved pharmacokinetics (PK) and efficacy relative to stochastic conjugates (15), likely due to the lack of under- and overconjugated species in the preparation, which can lead to ineffective or overly toxic molecules, respectively (16, 17). Furthermore, the noncleavable linker-maytansine payload used on our anti-CD22 ADC is resistant to efflux by MDR1 (18, 19) and does not mediate bystander killing. Together, these features likely contribute to the efficacy and safety of CAT-02-106 observed in preclinical studies.

Materials and Methods

General

All animal studies were conducted in accordance with Institutional Animal Care and Use Committee guidelines and were performed at Charles River Laboratories, Aragen Bioscience, or Covance Laboratories. The murine anti-maytansine antibody was made by ProMab and validated in-house. The rabbit anti-AF488 antibody was purchased from Life Technologies. The horseradish peroxidase (HRP)-conjugated secondary antibodies were from Jackson Immunoresearch. The antibodies used for pharmacodynamic studies were from BD Pharmingen. Cell lines were obtained from ATCC and DSMZ cell banks where they were authenticated by morphology, karyotyping, and PCR-based approaches. Cell lines have not been retested since beginning culture in our laboratory 2 years ago.

Cloning, expression, and purification of tagged antibodies

Antibodies were generated using standard cloning and purification techniques and GPEx expression technology as described previously (20).

Bioconjugation, purification, and HPLC analytics

ADCs were made and characterized as described previously (14).

Generation of MDR1$^+$ cell lines

MDR1 (ABCB1) cDNA was obtained from Sino Biological and cloned into a pEF plasmid with a hygromycin selection marker. An AMAXA Nucleofector instrument was used to electroporate Ramos (ATCC CRL-1923) and WSU-DLCL2 (DSMZ ACC 575) cells according to the manufacturer's recommendations. After selection with hygromycin (Invitrogen 10687010), the pools were enriched with paclitaxel treatment (25 nmol/L for up to 10 days) to further select cells with functional MDR1. The resulting cells were maintained under hygromycin selection in RPMI (Gibco 21870-092) supplemented with 10% fetal bovine serum (FBS) and 1X GlutaMax (Gibco 35050-079).

In vitro cytotoxicity assays

Cell lines were plated in 96-well plates (Costar 3610) at a density of 5×10^4 cells/well in 100 μL of growth media and allowed to rest for 5 hours. Serial dilution of test samples was performed in RPMI at 6× the final concentration and 20 μL was added to the cells. After incubation at 37°C with 5% CO_2 for 5 days, viability was measured using a Promega CellTiter 96 AQueous One Solution Cell Proliferation Assay (G3581) according to the manufacturer's recommendations. GI_{50} curves were calculated in GraphPad Prism using the ADC's drug-to-antibody ratio (DAR) value to normalize the dose to the payload concentration.

Xenograft studies

Female CB17 ICR SCID mice were inoculated subcutaneously with either WSU-DLCL2 or Ramos cells in 50% Matrigel. Tumors were measured twice weekly and tumor volume was estimated according to the formula: tumor volume $(\text{mm}^3) = \frac{w^2 x l}{2}$ where w is tumor width and l is tumor length. When tumors reached the desired mean volume, animals were randomized into groups of 8 to 12 mice and were dosed as described in the text. Animals were euthanized at the end of the study or when tumors reached 2000 mm^3.

Rat toxicology study and toxicokinetic (TK) analysis

Male Sprague-Dawley rats (8–9 week old at study start) were given a single intravenous dose of 6, 20, 40, or 60 mg/kg of CAT-02-106 (5 animals/group). Animals were observed for 12 days after dose. Body weights were recorded on days 0, 1, 4, 8, and 11. Blood was collected from all animals at 8 hours and at 5, 9, and 12 days and was used for TK analyses (all time points) and for clinical chemistry and hematology analyses (days 5 and 12). TK analyses were performed by ELISA, using the same conditions and reagents as described for the PK analyses.

Nonhuman primate toxicology and TK studies

Cynomolgus monkeys (2/sex/group) were given two doses (every 21 days) of 10, 30, or 60 mg/kg of CAT-02-106 followed by a 21-day observation period. Body weights were assessed prior to dosing on day 1, and on days 8, 15, 22 (predose), 29, 36, and 42. Blood was collected for TK, clinical chemistry, and hematology analyses according to the schedules presented in Supplementary Table S1. TK analyses were performed by ELISA, using the same conditions and reagents as described for the PK analyses, except that CD22-His protein was used as the capture reagent for the total antibody and total ADC measurements.

PK study designs

For the mouse study, animals used in the Ramos xenograft experiment were sampled in groups of three at time points beginning at 1 hour after first dose and continuing across the observation period. For the rat study, male Sprague-Dawley rats (3 per group) were dosed intravenously with a single 3 mg/kg bolus

of ADC. Plasma was collected at 1 hour, 8 hours, and 24 h, and 2, 4, 6, 8, 10, 14, and 21 days after dose. Plasma samples were stored at −80°C until use.

PK and TK sample analysis

The concentrations of total antibody, total ADC (DAR-sensitive), and total conjugate (DAR ≥1) were quantified by ELISA as diagrammed in Supplementary Fig. S1. For total antibody, conjugates were captured with an anti-human IgG-specific antibody and detected with an HRP-conjugated anti-human Fc-specific antibody. For total ADC, conjugates were captured with an anti-human Fab-specific antibody and detected with a mouse anti-maytansine primary antibody, followed by an HRP-conjugated anti-mouse IgG-subclass 1-specific secondary antibody. For total conjugate, conjugates were captured with an anti-maytansine antibody and detected with an HRP-conjugated anti-human Fc-specific antibody. Bound secondary antibody was detected using Ultra TMB One-Step ELISA substrate (Thermo Fisher). After quenching the reaction with sulfuric acid, signals were read by taking the absorbance at 450 nm on a Molecular Devices Spectra Max M5 plate reader equipped with SoftMax Pro software. Data were analyzed using GraphPad Prism and Microsoft Excel software.

Results and Discussion

Production and initial characterization of CAT-02-106

The anti-CD22 antibody that we used (CAT-02) is a humanized variant of the RFB4 antibody (21). *C*-terminally tagged anti-CD22 antibody was made as previously described (14, 20) using a GPEx clonal cell line with bioreactor titers of 1.6 g/L and 97% conversion of cysteine to formylglycine. The HIPS-4AP-maytansine linker payload (RED-106) was synthesized (Supplementary methods) and conjugated to the aldehyde-tagged antibody as previously described (14). The resulting ADC, CAT-02-106, was characterized (Supplementary Fig. S2) by size exclusion chromatography to assess percent monomer (99.2%), and by hydrophobic interaction (HIC) and reversed-phase (PLRP) chromatography to assess the drug-to-antibody ratio (DAR), which was 1.8. The ADC was compared with the wild-type (untagged) anti-CD22 antibody in terms of affinity for human CD22 protein and internalization on $CD22^+$ cells using an ELISA-based method (Supplementary Fig. S3) and a flow cytometric–based method (Supplementary Fig. S4), respectively. For both functional measures, the ADC performed equally well as the wild-type antibody, indicating that conjugation had no effect on these parameters.

CAT-02-106 is not a substrate for MDR1 and does not promote off-target or bystander killing

Potency of CAT-02-106 was tested *in vitro* against the Ramos and WSU-DLCL2 NHL tumor cell lines. Activity was compared with that of free maytansine, and a related ADC was made with the CAT-02 anti-CD22 antibody conjugated to maytansine through a cleavable valine–citrulline dipeptide linker (22). Both ADCs showed subnanomolar activity against wild-type Ramos and WSU-DLCL2 cells (Fig. 1A and C). In variants of those cells engineered to express the xenobiotic efflux pump, MDR1, only CAT-02-106 retained its original potency (Fig. 1B and D). By contrast, free maytansine was ∼10-fold less efficacious, and the ADC bearing cleavable maytansine was essentially devoid of activity. In a control experiment, cotreatment of WSU-DLCL2 cells with cyclosporin, an MDR1 inhibitor, had no effect on wild-type cells but restored the original potency of free maytansine and the cleavable ADC in $MDR1^+$ cells (Fig. 1E and F). Together, these results suggested that the active metabolite of CAT-02-106 was not a substrate for MDR1 efflux. In related *in vitro* cytotoxicity studies, CAT-02-106 had no effect on the antigen-negative cell line, NCI-N87 (Supplementary Fig. S5), indicating that it had no off-target activity up to 100 nmol/L over a 5-day cell culture period. Furthermore, an anti–HER2-based ADC conjugated to RED-106 did not mediate bystander killing of antigen-negative cells in coculture with antigen-positive cells (Supplementary Fig. S6), implying that the active metabolite of CAT-02-106—which would be the same as that of the anti-HER2 RED-106 conjugate—would also not mediate bystander killing.

CAT-02-106 is efficacious against NHL xenograft models

The *in vivo* efficacy of CAT-02-106 was assessed against the WSU-DLCL2 and Ramos xenograft models, which express relatively higher and lower amounts of CD22, respectively (Supplementary Fig. S7 and ref. 9). The resulting efficacy data are presented as either the mean or the individual animal tumor volumes in Fig. 2 and Supplementary Fig. S8, respectively. In a single dose study, mice bearing WSU-DLCL2 tumors were given 10 mg/kg of CAT-02-106 or a vehicle control. Dosing was initiated when the tumors averaged 118 mm^3. Of the animals that received the ADC, 25% (2 of 8) had a partial response, with tumors that had regressed to 4 mm^3 by day 31. The CAT-02-106–treated and vehicle control groups had mean tumor volumes of 415 and 1783 mm^3, respectively, by day 31. Next, in a multidose study, mice bearing WSU-DLCL2 xenografts were treated with 10 mg/kg of CAT-02-106 or a vehicle control every 4 days for a total of 4 doses. Dosing was initiated when the tumors averaged 262 mm^3. Of the animals that received the ADC, 75% (6 of 8) showed a complete response, with 38% of these (3 of 8) durable to the end of the study (day 59), 43 days after the last dose. By contrast, the vehicle control group reached a mean tumor volume of 2,191 mm^3 by day 17. Finally, in a multidose study, mice bearing Ramos xenografts were treated with either 5 or 10 mg/kg of CAT-02-106 or a vehicle control every 4 days for a total of 4 doses. Dosing was initiated when the tumors averaged 246 mm^3. As anticipated, a dose effect was observed with the groups receiving the 5 or 10 mg/kg dose demonstrating 63% or 87% tumor growth delay, respectively. Specifically, the median times to endpoint were 12, 19, and 22 days for the vehicle control, 5-, and 10-mg/kg dosing groups, respectively. In all three studies, no effect was observed on mouse body weight in the CAT-02-106 dosing groups (Supplementary Fig. S9).

CAT-02-106 is well tolerated at up to 60 mg/kg in rats and cynomolgus monkeys

CAT-02-106 does not bind to rodent CD22; however, dosing the ADC in these animals can provide information related to off-target toxicity and safety of the linker payload. As mentioned above, in mouse xenograft studies no effect of dosing was observed on body weight or clinical observations. In an exploratory rat toxicity study (Fig. 3), animals (5 per group) were given a single intravenous dose of CAT-02-106 at 6, 20, 40, or 60 mg/kg and observed for 12 days after dose. All

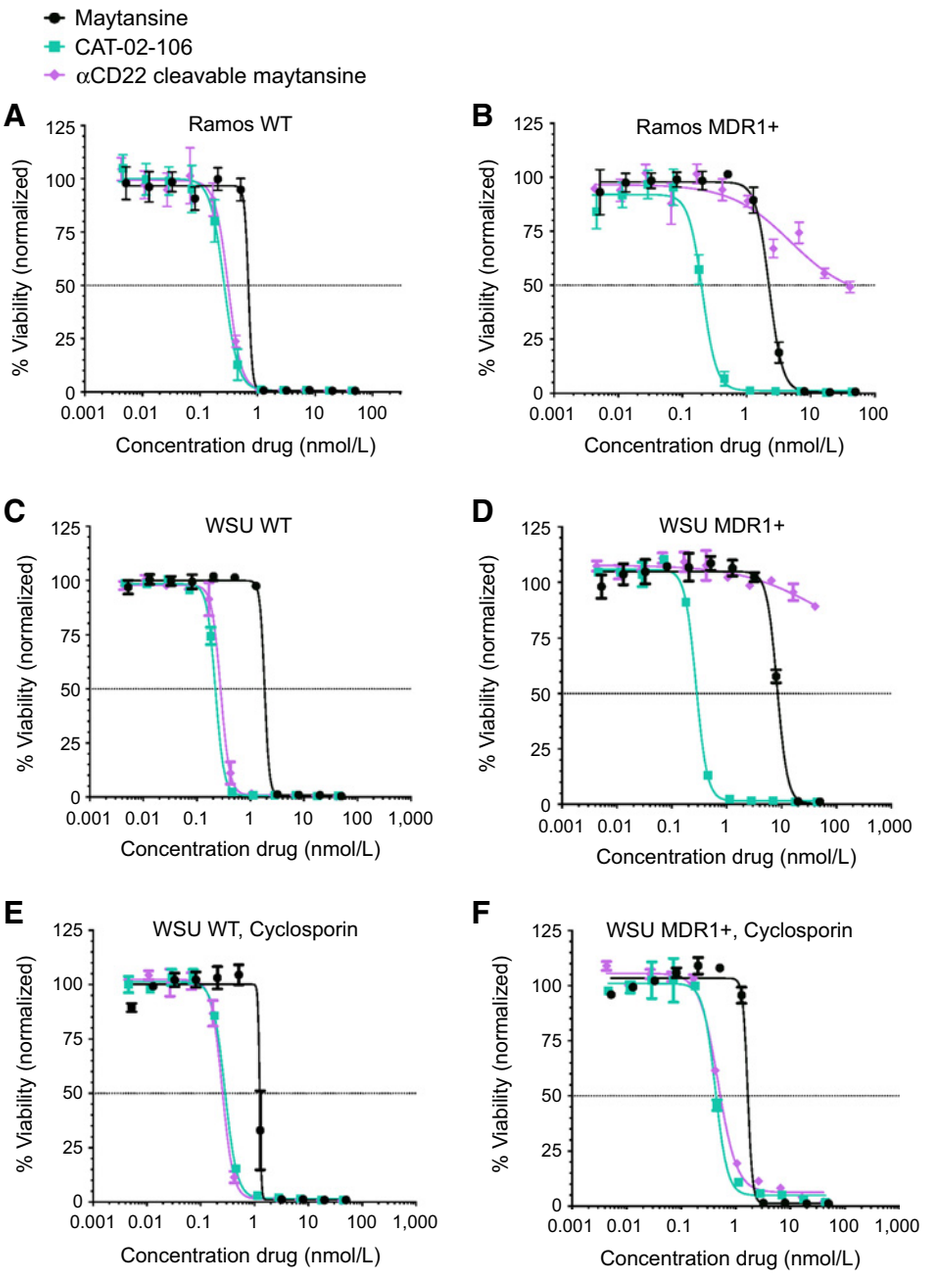

Figure 1.
CAT-02-106 is equally potent against parental and MDR1-expressing NHL tumor cells *in vitro*. Ramos and WSU-DLCL2 parental (WT) cells (**A** and **C**) and variants of those lines that were engineered to express MDR1 (MDR1$^+$, **B** and **D**) were used as targets for *in vitro* cytotoxicity studies of CAT-02-106 activity. Free maytansine and an αCD22 ADC made with the CAT-02 antibody but conjugated to maytansine using a valine–citrulline cleavable linker were used as controls. In an additional control experiment, the MDR1 inhibitor, cyclosporin, was added to WT or MDR1$^+$ WSU-DLCL2 cells (**E** and **F**). The data are presented as the mean ± SD ($n = 2$).

animals survived until the end of the study. Animals dosed at 60 mg/kg experienced a 10% decrease in body weight relative to the vehicle control group. Clinical chemistry changes compatible with minimal to mild hepatobiliary injury occurred on day 5 in animals given ≥40 mg/kg and consisted of increased activities of alanine aminotransferase (ALT), aspartate transaminase (AST), and alkaline phosphatase. Most changes had reversed by day 12. With respect to hematology, moderately to markedly decreased platelet counts occurred on day 5 in animals given ≥40 mg/kg and had completely reversed by day 12. Changes compatible with inflammation occurred on days 5 and 12 in animals given ≥40 mg/kg and consisted of slightly to moderately increased neutrophil and monocyte counts, slightly increased globulin concentrations, and decreased albumin: globulin ratio.

CAT-02-106 does bind to cynomolgus CD22 (Supplementary Fig. S10) and has a similar tissue cross-reactivity profile in monkeys as compared with humans (Supplementary Fig. S11). Therefore, cynomolgus monkeys represent an appropriate model in which to test both the on-target and off-target toxicities of this ADC. In an exploratory repeat dose study, monkeys (2/sex/group) were given 10, 30, or 60 mg/kg of CAT-02-106 once every 3 weeks for a total of 2 doses followed by a 21-day observation period. All animals survived until study termination. No CAT-02-106–

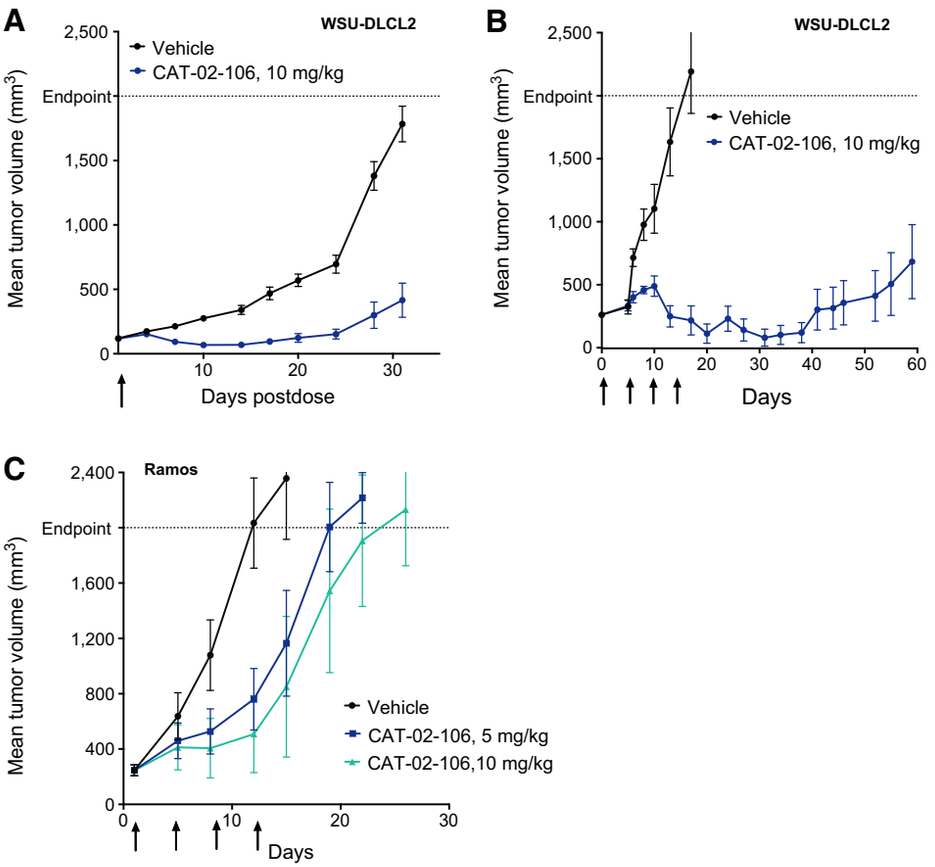

Figure 2.
CAT-02-106 is efficacious *in vivo* against the NHL-derived WSU-DLCL2 and Ramos xenograft models. Female CB17 ICR SCID mice (8/group) bearing WSU-DLCL2 xenografts were treated with vehicle alone or with CAT-02-106 as either a (**A**) single 10 mg/kg dose or (**B**) as multiple 10 mg/kg doses delivered every four days for a total of four doses (q4d × 4). Treatment was initiated when tumors reached an average size of 118 or 262 mm^3 for the single or multidose studies, respectively. **C,** Female CB17 ICR SCID mice (12/group) bearing Ramos xenografts were treated with vehicle alone, or with 5 or 10 mg/kg CAT-02-106 q4d × 4. Dosing was initiated when tumors reached an average size of 246 mm^3. The data are presented as the mean ± SEM.

related changes in clinical observations, body weights, or food consumption occurred. Clinical pathology changes occurred mostly in animals given ≥30 mg/kg and were consistent with minimal liver injury, increased platelet consumption and/or sequestration, and inflammation (Fig. 4). These changes were similar at 30 and 60 mg/kg and after the first and second doses, and were of a magnitude that would not be expected to be associated with microscopic changes or clinical effects. Changes compatible with minimal liver injury in animals given ≥30 mg/kg consisted of increased ALT, AST, and ALP activities that had

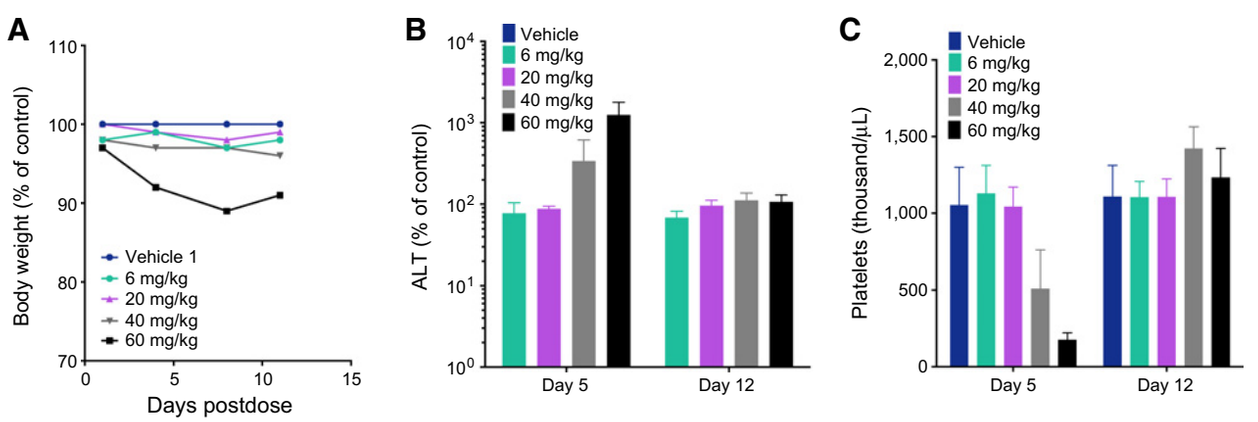

Figure 3.
CAT-02-106 can be dosed in rats up to 60 mg/kg with minimal effects. Sprague-Dawley rats (5/group) received a 6, 20, 40, or 60 mg/kg dose of CAT-02-106 followed by a 12-day observation period. **A,** Body weight was monitored at the times indicated. **B,** ALT and (**C**) platelet counts were assessed at 5 and 12 days after dose. The data are presented as the mean ± SD.

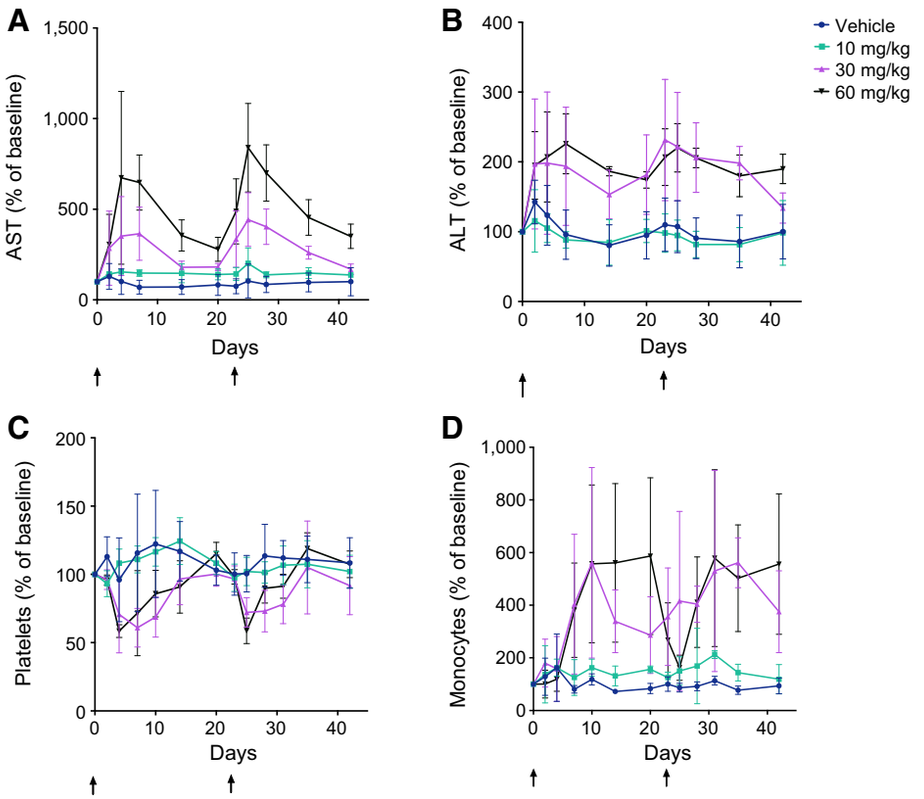

Figure 4.
Cynomolgus monkeys display no observed adverse effects with a repeat 60 mg/kg dose of CAT-02-106. Cynomolgus monkeys (2/sex/group) were given 10, 30, or 60 mg/kg of CAT-02-106 once every three weeks for a total of two doses followed by a 21-day observation period. **A,** AST, (**B**) ALT, (**C**) platelets, and (**D**) monocytes were monitored at the times indicated. The data are presented as the mean ± SD.

partially reversed by days 21 and 42. Slightly to moderately decreased platelet counts observed within a week of dosing had mostly reversed by days 21 and 42. Changes compatible with inflammation consisted of minimally to moderately increased neutrophil and monocyte counts, slightly to moderately increased globulin concentrations, and minimally decreased albumin concentrations.

Pharmacokinetics and toxicokinetics of CAT-02-106 in mice, rats, and cynomolgus monkeys

In order to evaluate the *in vivo* stability of CAT-02-106, we conducted a PK study in rats. We monitored the concentrations of total antibody, total ADC, and total conjugate in the peripheral blood of animals (3/group) for 21 days after receiving a single 3 mg/kg dose of CAT-02-106 (Supplementary Table S1 and Fig. 5). As shown in Supplementary Fig. S1, the total ADC and total conjugate assays use DAR-sensitive and DAR-insensitive measurements, respectively. The PK parameters obtained for all three analytes were similar, indicating that the conjugate was largely stable in circulation. For example, the elimination half-lives of total antibody, total ADC, and total conjugate were 9.48, 6.13, and 7.22 days, respectively.

Next, we measured CAT-02-106 analyte concentrations over time in the peripheral blood of mice from the Ramos multidose efficacy study described above. The purpose of this analysis was to determine the total ADC exposure level achieved at an efficacious dose in xenograft studies (Table 1). For this benchmark, recall that 10 mg/kg × 4 doses over 22 days led to an 87% tumor growth delay in the Ramos model, and that 10 mg/kg × 4 doses over 28 days led to 75% of the animals exhibiting a complete response (no palpable tumor remaining) in the WSU-DLCL2 model. The mean area under the concentration versus time curve from time 0 to infinity ($AUC_{0\text{-inf}}$) for the 10 mg/kg × 4 dose in the mouse was 2,530 ± 131 (S.D.) day · μg/mL.

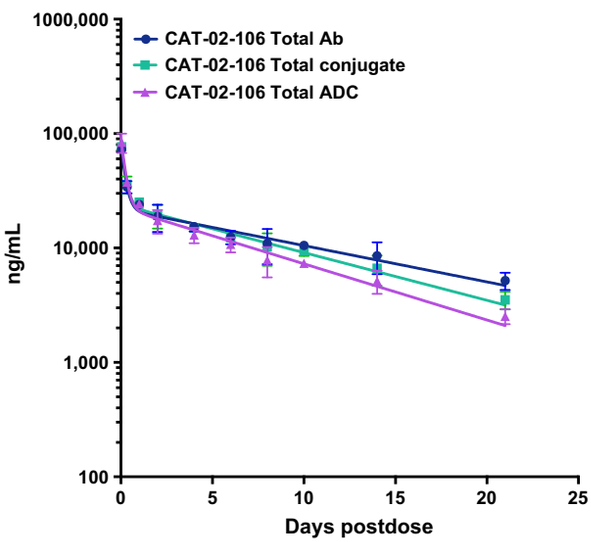

Figure 5.
CAT-02-106 displays very high *in vivo* stability as exemplified by a rat PK study. Sprague-Dawley rats (3/group) were given a single i.v. bolus dose of 3 mg/kg CAT-02-106. Plasma samples were collected at the designated times and were analyzed (as shown in Supplementary Fig. S1) for total antibody, total conjugate, and total ADC concentrations.

Table 1. Summary of mean (±SD) PK and TK parameters of total ADC values in animals dosed with CAT-02-106

	Mouse (q4d × 4)[a]		Rat (single dose)		Cynomolgus monkey (q3w × 2)[b]	
Dose (mg/kg)	$C_{max\ first\ dose}$ (μg/mL)	$AUC_{0\text{-}inf}$ (day·μg/mL)	C_{max} (μg/mL)	$AUC_{0\text{-}inf}$ (day·μg/mL)	$C_{max\ first\ dose}$ (μg/mL)	$AUC_{0\text{-}inf}$ (day·μg/mL)
3			83.9 (16)	218 (18.4)		
5	74.4 (5.48)	1,500 (45.1)				
6			110 (38.5)	660 (143)		
10	136 (4.57)	2,530 (131)			318 (110)	1,360 (556)
20			382 (63.0)	2,280 (325)		
30					1,030 (57.4)	4,200 (768)
40			687 (52.8)	3,740 (185)		
60			1,020 (158)	5,201 (273)	1,630 (138)	6,140 (667)

Abbreviations: $AUC_{0\text{-}inf}$, area under the concentration versus time curve from time 0 to infinity; C_{max}, highest concentration observed at the first sampling time point from each study as follows: mouse and rat PK, 1 hours; rat TK, 8 hours; cynomolgus TK, 5 minutes; SD, standard deviation.
[a]AUC calculation includes all doses.
[b]AUC calculation from the first dose only.

Finally, we assessed CAT-02-106 analyte concentrations in TK plasma samples from animals dosed in the previously described rat and cynomolgus monkey toxicity studies (Table 1). The purpose of these analyses was to determine the total ADC exposure levels achieved at doses correlated to the presence or absence of changes in clinical chemistry or hematology panels. For both the rat and monkey studies, the C_{max} and $AUC_{0\text{-}inf}$ values were generally proportional to the dose. The mean $AUC_{0\text{-}inf}$ for the 60 mg/kg dose was 5201 ± 273 day · μg/mL in rats and 6,140 ± 667 day · μg/mL in monkeys. The antibody does bind to antigen in the cynomolgus model. However, the dose proportional $AUC_{0\text{-}inf}$ values suggest that the low (10 mg/kg) dose was sufficient to saturate target-mediated clearance mechanisms, and therefore that antigen-mediated clearance did not significantly affect the results of this study.

Conclusions

We developed a CD22-targeted ADC site-specifically conjugated to a maytansine payload that was resistant to efflux by MDR1-expressing cells. The ADC, CAT-02-106, had a DAR of 1.8, displayed good biophysical characteristics, and mediated efficacy ranging from significant (87%) tumor growth delay to complete response *in vivo* against two NHL xenograft models. This efficacy was achieved at exposure levels well below those associated with toxicity; indeed, in the repeat dose cynomolgus toxicity study, no observed significant adverse effects were noted even at the highest dose of 60 mg/kg, opening the door to exploring even higher doses in future studies. The unique composition of matter defining CAT-02-106 confers its unusual combination of efficacy and safety. In particular, the novel HIPS-4AP noncleavable linker stands in contrast to the majority of linkers found in clinically tested ADCs (23), and likely drives much of the improvements observed in this construct. As an added advantage, a number of the ADC's other components—including the target antigen (24, 25), parental antibody (26), and the maytansine-based cytotoxic payload (27, 28)—have already been tested in humans and are known entities with respect to likely safety and toxicity issues. Presuming that the cynomolgus monkey is a reasonable model for projecting human PK and toxicity profiles (28, 29), CAT-02-106 could be of therapeutic use for NHL patients. In particular, patients that would likely benefit from CAT-02-106 treatment include those with disease that has become refractory to standard-of-care chemotherapies or to Besponsa treatment due to the upregulation of MDR1 (30–32).

Disclosure of Potential Conflicts of Interest

D. Rabuka has ownership interest (including patents) in Catalent Pharma Solutions. No potential conflicts of interest were disclosed by the other authors.

Authors' Contributions

Conception and design: P.M. Drake, J.M. McFarland, R. Kudirka, D. Rabuka
Development of methodology: P.M. Drake, J.M. McFarland, R.M. Barfield, W. Zmolek, B.C.B. Huang, R. Kudirka, D. Rabuka
Acquisition of data (provided animals, acquired and managed patients, provided facilities, etc.): P.M. Drake, A. Carlson, J.M. McFarland, S. Bañas, W. Zmolek, Y.C. Kim, B.C.B. Huang, R. Kudirka
Analysis and interpretation of data (e.g., statistical analysis, biostatistics, computational analysis): P.M. Drake, A. Carlson, W. Zmolek, Y.C. Kim, B.C.B. Huang, R. Kudirka, D. Rabuka
Writing, review, and/or revision of the manuscript: P.M. Drake, A. Carlson, D. Rabuka
Administrative, technical, or material support (i.e., reporting or organizing data, constructing databases): P.M. Drake, Y.C. Kim, D. Rabuka
Study supervision: P.M. Drake, R.M. Barfield, D. Rabuka

The costs of publication of this article were defrayed in part by the payment of page charges. This article must therefore be hereby marked *advertisement* in accordance with 18 U.S.C. Section 1734 solely to indicate this fact.

Received August 12, 2017; revised October 2, 2017; accepted October 27, 2017; published OnlineFirst November 15, 2017.

References

1. Howlander N, Noone AM, Krapcho M, Garshell J, Miller D, Altekruse SF, et al., editors. SEER Cancer Statistics Review [Internet]. National Cancer Institute; [cited 2016 May 5]. Available from: http://seer.cancer.gov/csr/1975_2012/.
2. Ferlay J, Soerjomataram I, Ervik M, Dikshit R, Eser S, Mathers C, et al., editors. GLOBOCAN 2012 v1.0 [Internet]. 11 ed. International Agency for Research on Cancer; [cited 2016 May 5]. Available from: http://globocan.iarc.fr.
3. Bray F, Ren J-S, Masuyer E, Ferlay J. Global estimates of cancer prevalence for 27 sites in the adult population in 2008. Int J Cancer 2013;132:1133–45.
4. Ferlay J, Soerjomataram I, Dikshit R, Eser S, Mathers C, Rebelo M, et al. Cancer incidence and mortality worldwide: sources, methods and major patterns in GLOBOCAN 2012. Int J Cancer 2015;136:E359–86.
5. Advani A, Coiffier B, Czuczman MS, Dreyling M, Foran J, Gine E, et al. Safety, pharmacokinetics, and preliminary clinical activity of inotuzumab ozogamicin, a novel immunoconjugate for the treatment of B-cell non-

Hodgkin's lymphoma: results of a phase I study. J Clin Oncol 2010;28: 2085–93.
6. Weber T, Mavratzas A, Kiesgen S, Haase S, Bötticher B, Exner E, et al. A humanized anti-CD22-onconase antibody–drug conjugate mediates highly potent destruction of targeted tumor cells. J Immunol Res 2015;2015:1–14.
7. Shor B, Gerber H-P, Sapra P. Preclinical and clinical development of inotuzumab-ozogamicin in hematological malignancies. Mol Immunol 2015;67:107–16.
8. Kantarjian HM, DeAngelo DJ, Stelljes M, Martinelli G, Liedtke M, Stock W, et al. Inotuzumab ozogamicin versus standard therapy for acute lymphoblastic leukemia. N Engl J Med 2016;375:740–53.
9. Li D, Poon KA, Yu S-F, Dere R, Go M, Lau J, et al. DCDT2980S, an anti-CD22-monomethyl auristatin E antibody–drug conjugate, is a potential treatment for non-Hodgkin lymphoma. Mol Cancer Ther 2013;12:1255–65.
10. Morschhauser F, Flinn I, Advani RH, Diefenbach CS, Kolibaba K, Press OW, et al. Updated results of a phase II randomized study (ROMULUS) of polatuzumab vedotin or pinatuzumab vedotin plus rituximab in patients with relapsed/refractory non-Hodgkin lymphoma. Blood 2014; 124:4457–7.
11. Rabuka D, Rush JS, deHart GW, Wu P, Bertozzi CR. Site-specific chemical protein conjugation using genetically encoded aldehyde tags. Nat Protoc 2012;7:1052–67.
12. Agarwal P, Kudirka R, Albers AE, Barfield RM, de Hart GW, Drake PM, et al. Hydrazino-pictet-spengler ligation as a biocompatible method for the generation of stable protein conjugates. Bioconjug Chem 2013;24:846–51.
13. Holder PG, Jones LC, Drake PM, Barfield RM, Banas S, deHart GW, et al. Reconstitution of formylglycine-generating enzyme with copper (II) for aldehyde tag conversion. J Biol Chem 2015;290:15730–45.
14. Drake PM, Albers AE, Baker J, Banas S, Barfield RM, Bhat AS, et al. Aldehyde tag coupled with HIPS chemistry enables the production of ADCs conjugated site-specifically to different antibody regions with distinct *in vivo* efficacy and PK outcomes. Bioconjug Chem 2014;25:1331–41.
15. Junutula JR, Raab H, Clark S, Bhakta S, Leipold DD, Weir S, et al. Site-specific conjugation of a cytotoxic drug to an antibody improves the therapeutic index. Nat Biotechnol 2008;26:925–32.
16. Hamblett KJ, Senter PD, Chace DF, Sun MMC, Lenox J, Cerveny CG, et al. Effects of drug loading on the antitumor activity of a monoclonal antibody drug conjugate. Clin Cancer Res 2004;10:7063–70.
17. Strop P, Delaria K, Foletti D, Witt JM, Hasa-Moreno A, Poulsen K, et al. Site-specific conjugation improves therapeutic index of antibody drug conjugates with high drug loading. Nat Biotechnol 2015;33:694–6.
18. Kovtun YV, Audette CA, Mayo MF, Jones GE, Doherty H, Maloney EK, et al. Antibody–maytansinoid conjugates designed to bypass multidrug resistance. Cancer Res 2010;70:2528–37.
19. Hong EE, Chari R. AAPS Advances in the Pharmaceutical Sciences Series. In: Wang J, Shen W-C, Zaro JL, editors. AAPS Advances in the Pharmaceutical Sciences Series 2210-73712210-738X. Cham: Springer International Publishing; 2015. p.153–75.
20. York D, Baker J, Holder PG, Jones LC, Drake PM, Barfield RM, et al. Generating aldehyde-tagged antibodies with high titers and high formylglycine yields by supplementing culture media with copper(II). BMC Biotechnol 2016;16:23.
21. Li JL, Shen GL, Ghetie MA, May RD, Till M, Ghetie V, et al. The epitope specificity and tissue reactivity of four murine monoclonal anti-CD22 antibodies. Cell Immunol 1989;118:85–99.
22. Doronina SO, Mendelsohn BA, Bovee TD, Cerveny CG, Alley SC, Meyer DL, et al. Enhanced activity of monomethylauristatin F through monoclonal antibody delivery: effects of linker technology on efficacy and toxicity. Bioconjug Chem 2006;17:114–24.
23. Beck A, Goetsch L, Dumontet C, Corvaïa N. Strategies and challenges for the next generation of antibody–drug conjugates. Nat Rev Drug Discov 2017;16:315–37.
24. Pfeifer M, Zheng B, Erdmann T, Koeppen H, McCord R, Grau M, et al. Anti-CD22 and anti-CD79B antibody drug conjugates areactive in different molecular diffuse large B-cell lymphoma subtypes. Leukemia 2015;29: 1578–86.
25. Ogura M, Hatake K, Ando K, Tobinai K, Tokushige K, Ono C, et al. Phase I study of anti-CD22 immunoconjugate inotuzumab ozogamicin plus rituximab in relapsed/refractory B-cell non-Hodgkin lymphoma. Cancer Sci 2012;103:933–8.
26. Wayne AS, Kreitman RJ, Findley HW, Lew G, Delbrook C, Steinberg SM, et al. Anti-CD22 immunotoxin RFB4(dsFv)-PE38 (BL22) for CD22-positive hematologic malignancies of childhood: preclinical studies and phase I clinical trial. Clin Cancer Res 2010;16:1894–903.
27. Amiri-Kordestani L, Blumenthal GM, Xu QC, Zhang L, Tang SW, Ha L, et al. FDA approval: ado-trastuzumab emtansine for the treatment of patients with HER2-positive metastatic breast cancer. Clin Cancer Res 2014;20: 4436–41.
28. Saber H, Leighton JK. An FDA oncology analysis of antibody–drug conjugates. Regul Toxicol Pharmacol 2015;71:444–52.
29. Oitate M, Nakayama S, Ito T, Kurihara A, Okudaira N, Izumi T. Prediction of human plasma concentration-time profiles of monoclonal antibodies from monkey data by a species-invariant time method. Drug Metab Pharmacokinet 2012;27:354–9.
30. Andreadis C, Gimotty PA, Wahl P, Hammond R, Houldsworth J, Schuster SJ, et al. Members of the glutathione and ABC-transporter families are associated with clinical outcome in patients with diffuse large B-cell lymphoma. Blood 2007;109:3409–16.
31. Svoboda-Beusan I, Kusec R, Bendelja K, Tudoric-Ghemo I, Jaksic B, Pejsa V, et al. The relevance of multidrug resistance-associated P-glycoprotein expression in the treatment response of B-cell chronic lymphocytic leukemia. Haematologica 2000;85:1261–7.
32. Takeshita A, Shinjo K, Yamakage N, Ono T, Hirano I, Matsui H, et al. CMC-544 (inotuzumab ozogamicin) shows less effect on multidrug resistant cells: analyses in cell lines and cells from patients with B-cell chronic lymphocytic leukaemia and lymphoma. Br J Haematol 2009;146:34–43.